*Desalination and Water Treatment*
www.deswater.com

doi: 10.5004/dwt.2022.28690

267 (2022) 98–107
August

# Effective removal of phosphate from solution by iron-doped chitosan/polyvinyl alcohol composite membrane

Ruize Zhang, Kang Wen*, Runping Han*

*College of Chemistry, Green Catalysis Center, Zhengzhou University, No. 100 of Kexue Road, Zhengzhou 450001, China, emails: 1039171416@qq.com (K. Wen), rphan67@zzu.edu.cn (R. Han), 690724768@qq.com (R. Zhang)*

Received 18 February 2022; Accepted 6 July 2022

**ABSTRACT**

One Fe-doped blended membrane (CS-Fe-PVA) prepared by doping polyvinyl alcohol and chitosan with $FeCl_3 \cdot 6H_2O$ was applied as an adsorbent for the removal of phosphates from solution. The characterization of CS-Fe-PVA was performed using X-ray photoelectron spectroscopy (XPS) and scanning electron microscope techniques whereas the adsorption studies were carried out via the batch mode. CS-Fe-PVA exhibited high stability in acidic medium with an improved adsorption capacity which was attributed to the presence of $Fe^{3+}$ in the membrane. Results from the experiments showed that CS-Fe-PVA had an adsorption quantity of 29.8 mg $g^{-1}$ (as P) at 293 K. The Langmuir model was a better fit for the equilibrium data whereas the kinetic adsorption process was better described by the pseudo-second-order kinetic model. Thermodynamic studies confirmed the adsorption process to be spontaneous and exothermic. The results from the XPS analysis as well as the adsorption experiments suggested that the coordination process is the major reaction mechanism for the uptake of phosphate onto CS-Fe-PVA. CS-Fe-PVA is potential to bind phosphate from solution.

*Keywords:* CS-Fe-PVA composite membranes; Adsorption; Phosphate

## 1. Introduction

Recent studies have shown that the deterioration of water quality by eutrophication is closely related to the presence of higher level of nitrogen and phosphorus nutrients (especially phosphate) in natural water [1,2]. When large amounts of nutrients enter the slow-flow watershed, more algae and other plankton can multiply rapidly, which decrease the level of oxygen content in the water body and lead to the death of fish and some plankton. This occurrence has the propensity of affecting some physicochemical properties of water such as pH, dissolved oxygen (DO) and carbon levels, thus can adversely affect the biological community and alter its biodiversity [3,4]. Due to these associated problems, several methods (including chemical treatment, physical treatment and biological treatment) have been developed for the removal of phosphorus from natural water [5,6]. Amongst these methods, adsorption has been significantly applied for the removal of phosphate from solution due to its simplicity, low-cost, efficiency and facile operations [7–9]. Furthermore, it is highly efficient in terms of energy consumption for large scale operations [10,11].

Chitin is a natural compound and the second most abundant biopolymer polysaccharide. Chitosan (a cationic polymer, with its main chemical structure composed of basic polysaccharide) is obtained from the deacetylation of chitin [12,13]. Chitosan contains amino groups and hydroxyl groups in its structure, which can bind some metal ions through coordination or chelation. At the same time, it can also be used to treat wastewater containing dyes and halogens through ion exchange, etc. Therefore, various adsorbents based on chitosan have been extensively applied for the removal of refractory pollutants and phosphate [14]. Nanocomposite of Zr-loaded chitosan/$Fe_3O_4$/graphene oxide was stable in water

* Corresponding authors.

and highly efficient for the sequestration of fluoride ion with selectivity [15]. Chitosan-polyacrylonitrile composite was synthesized using 5% glutaraldehyde (as a cross-linking agent) to remove lead from polluted water [16].

A cross-linking agent such as glutaraldehyde or epichlorohydrin can be used to ensure the stability of the chitosan composite. Also, the stability and mechanical properties of chitosan composite can be improved through doped metal ions [17]. This is attributed to the ability of heavy metal ions to bind with the functional groups present in chitosan to form a network structure. In addition, the composite still exhibits good adsorption capacity for the removal of some pollutants, even at higher electrolyte concentration [18].

Membrane materials are widely used in several fields because of their large contact area and easy fabrication process [19]. Furthermore, these spent adsorbents can be simply separated from the mixtures. Chitosan as the main material can be used to prepare membrane materials for the removal of phosphate from water [20,21]. However, there is poor mechanical strength while the membrane can be dissolved in weak acidic condition without cross-linking agent. To overcome these challenges, polyvinyl alcohol (PVA) is added to enhance the mechanical properties of the formed membrane [20]. Habiba et al. [22] also found that chitosan/(polyvinyl alcohol)/zeolite electrospun composite nanofibrous membrane exhibited significant removal efficiency for Cr(VI), $Fe^{3+}$ and $Ni^{2+}$ from solution. Zhou et al. [17] prepared the Fe-cross-linking chitosan complex, which had a good stability and higher adsorption capacity to 2,4-dichlorophenoxyacetic acid. Moreover, the stability and adsorption capacity of the adsorbent (iron-doped PVA-chitosan composite film) toward removing Congo red was improved by doping the adsorbent with trivalent iron to form a network structure [18].

In this study, Fe-doped blended membrane (CS-Fe-PVA) was prepared by doping polyvinyl alcohol and chitosan with $FeCl_3{\cdot}6H_2O$ and its efficiency for the removal of phosphates in solution was evaluated. The kinetics, equilibrium and thermodynamic properties are presented and mechanisms of adsorption are further discussed.

## 2. Materials and methods

### 2.1. Materials

Ferric chloride ($FeCl_3{\cdot}7H_2O$) and polyvinyl alcohol ($[CH_2CH(OH)]_n$) (Fengchuan Chemical Reagent Co. Ltd., Tianjin, China); chitosan ($(C_6H_{11}NO_4)_n$, Company of Chemical Reagent of Traditional Chinese Medicine, deacetylation degree >95%, CAS 9012-76-4, molecular weight $50 \times 10^4$ g $mol^{-1}$); potassium phosphate monobasic ($KH_2PO_4$, Chemical Company, Beijing) were all obtained from the manufacturers. All solutions used in the experiment were prepared by diluting standard stock solution with a certain volume of deionized water. All agents were of analytical grade.

### 2.2. Preparation of chitosan-polyvinyl alcohol-iron composite membrane (CS-Fe-PVA)

The composite membrane (CS-Fe-PVA) was prepared according to our previous reported method [18]. In brief, 3% chitosan solution and 4% polyvinyl alcohol solution were prepared, in which chitosan is dissolved by 5% acetic acid and polyvinyl alcohol is dissolved by deionized water. Chitosan solution and polyvinyl alcohol solution were mixed according to the mass ratio of 2:1. The $FeCl_3$ solution (0.3 mol $L^{-1}$) was added into the mixed solution to obtain membranes casting solution (the mass ratio of CS solution to trivalent iron solution was 3:1). The liquid of casting membranes was added to a specific casting membranes machine and heated in an oven until the membranes were separated from the casting membranes machine. The composite membrane was then immersed in 5% (w/w) NaOH solution for 10 min after which the membrane was taken out from the solution and washed with deionized water to neutral pH. The film was dried in shade at room temperature and the blend composite membrane (CS-Fe-PVA) was obtained.

### 2.3. Characterization of CS-Fe-PVA

To further study the mechanism associated with the uptake of phosphates onto CS-Fe-PVA, the surface morphology and related groups of CS-Fe-PVA were explored. The point of zero charge ($pH_{pzc}$) of CS-Fe-PVA was determined by measuring a series of changes in pH value of 0.1 mol $L^{-1}$ sodium chloride solutions. The dried samples obtained after drying CS-Fe-PVA and CS-PVA in an oven at 373 K for 2 h, were cut and ground into small pieces. Then after, a small amount of CS-Fe-PVA and CS-PVA samples were uniformly adhered to the conductive adhesive. Prior to analysis, CS-Fe-PVA and CS-PVA samples (sprayed with gold) were dried in an oven for about 12 h. The surface property of CS-Fe-PVA was observed using scanning electron microscope (SEM) (Hitachi S-4800, Japan). The changes in the main functional groups before and after phosphate adsorption were studied using Fourier-transform infrared spectroscopy (Nicolet iS50, USA). The binding modes of the main functional groups of CS-Fe-PVA were analyzed using X-ray photoelectron spectroscopy (XPS) (ESCALAB 250Xi, UK).

### 2.4. Adsorption experiments

The influencing factors on $PO_4^{3-}$ adsorption by CS-Fe-PVA from aqueous solution were studied in batch mode. Briefly, 10 mg CS-Fe-PVA and 10 mL phosphate solution (30 mg $L^{-1}$) were put into conical flasks (50 mL), and shaken in a water bath at 120 rpm at 293 K. The effect of solution pH and the initial concentration of $Na_2SO_4$ and $NaNO_3$ on adsorption quantity were performed. The concentration of $PO_4^{3-}$ in solution was measured using the UV-Vis spectrophotometer at the wavelength of 700 nm by molybdenum antimony anti-spectrophotometry. The adsorption experiments were performed twice and the averages were recorded (error less than 5%).

The unit adsorption quantity ($q_t$ or $q_e$) of $PO_4^{3-}$ on CS-Fe-PVA was obtained using the expression:

$$q = \frac{V\left(C_0 - C\right)}{m} \tag{1}$$

where $C$ is the phosphate concentration (according to P) at any time or adsorption equilibrium and $C_0$ is the initial

phosphate concentration (mg $L^{-1}$); $m$ is the dosage of CS-Fe-PVA (mg); $V$ is the volume of the $PO_4^{3-}$ used in the adsorption process (L).

### 2.5. Equilibrium study

10 mL of $PO_4^{3-}$ solution (5–45 mg $L^{-1}$) were added to each series of conical flasks containing 10 mg CS-Fe-PVA. The experimental temperature of the oscillator was adjusted to 293, 303 and 313 K. The sealed conical flask with its content was placed in an oscillator for 2 h, after which the adsorbent was retrieved and the residual $PO_4^{3-}$ concentration was measured. The obtained adsorption data were fitted with the Langmuir model and Temkin model.

Langmuir equation is as follows:

$$q_e = \frac{q_m K_L C_e}{1 + K_L C_e} \tag{2}$$

Temkin equation is as follows:

$$q_e = A + B \ln C_e \tag{3}$$

where $q_m$ is the maximum adsorption amount that can be achieved by Langmuir model fitting (mg $g^{-1}$), $K_L$ is the equilibrium constant related to adsorption (L $mg^{-1}$), $A$ and $B$ are the adsorption constants related to Temkin model.

### 2.6. Kinetic studies

10 mg of CS-Fe-PVA were added to conical flasks containing 10 mL $PO_4^{3-}$ solutions at known concentrations (10, 20 and 30 mg $L^{-1}$), then the flasks were placed in an oscillator at three different temperatures (i.e., 293, 303 and 313 K). An aliquot from the respective conical flasks with different concentrations in continuous time was taken and the $PO_4^{3-}$ concentration in the solution was determined. Kinetic models *vis-à-vis* double constant equation, pseudo-second-order kinetic model and Elovich equation models were used to fit the data.

Double constant equation is as follows:

$$q_t = A t^{K_s} \tag{4}$$

Pseudo-second-order kinetic model is as follows:

$$q_t = \frac{k_2 q_e^2 t}{1 + k_2 q_e t} \tag{5}$$

Elovich equation is as follows:

$$q_t = A + B \ln t \tag{6}$$

where $q_e$ is the adsorption capacity at equilibrium and $q_t$ is $q_e$ under the fitting of the model at a certain time (mg $g^{-1}$); $A$ is the constant related to adsorption; $K_s$ is the correlation coefficient corresponding to the adsorption rate; $k_2$ is the rate constant corresponding to the quasi-second-order kinetic models (g $mg^{-1}$ $min^{-1}$); Both $A$ and $B$ in Eq. (6) are the parameters of Elovich equation.

### 2.7. Desorption experiment

The spent or exhausted CS-PVA-Fe was obtained from the phosphate adsorption performed at the initial concentration and temperature of 30 mg $L^{-1}$ and 303 K, respectively. The P-loaded CS-PVA-Fe was washed with distilled water to remove residual $PO_4^{3-}$ (not bonded) and dried at 333 K. The adsorbent was regenerated using 10 mL of 0.1 mol $L^{-1}$ NaOH solution for 60 min. The regenerated adsorbent was reused for adsorption studies under the same experimental conditions.

## 3. Result and analysis

### 3.1. Characterization of CS-Fe-PVA

#### 3.1.1. SEM and mapping analysis

In the previous study, SEM and mapping of CS-Fe-PVA were performed [18]. The surface morphology of CS-PVA was relatively smooth while that of CS-Fe-PVA was several wrinkles. This might be due to the coordination of $Fe^{3+}$ and $-NH_2$ on the surface of chitosan, which contributed to the change of the smooth surface nature of CS-PVA. Even distribution of Fe was observed in the membrane materials, which further proves that $Fe^{3+}$ was successfully combined with CS-PVA. Through the analysis of the local mapping of C and O (Fig. 1a and b), both elements were observed to be distributed on the surface of the material.

#### 3.1.2. XPS analysis

For the element confirmation and study of mechanism, XPS analysis is performed and the results are depicted in Fig. 2. Fig. 2a shows the energy spectrum of XPS for CS-Fe-PVA and P-loaded CS-Fe-PVA. Peaks at binding energy of 399.1, 285.6, 532.4 and 711.1 eV are corresponding to N 1s, C 1s, O 1s and Fe 2p, respectively [18]. It is also clearly observed from Fig. 2a that a new peak at 132.0 eV corresponding to the P 2p peak is recorded in the XPS spectrum of P-loaded CS-Fe-PVA. Therefore, it can be concluded that $PO_4^{3-}$ was successfully adsorbed onto the composite membranes.

The change in the O 1s peak value before and after adsorption can be observed in Fig. 2b and c. The peaks at 529.5 and 530.7 eV are ascribed to Fe–O and Fe–OH, which confirms the presence of metal oxides [23]. The peak shifts from 530.7 eV (Fe–O) to 530.1 eV (Fe–O–P) after adsorption, while the peak with low intensity at 529.5 eV is disappeared. The reason may be that the level of O (M–O) in adsorbent decreases after phosphate adsorption. This leads to the peak to be masked by the broad peak of O–Fe–P. The peaks at 532.6 and 532.4 eV are ascribed to $H_2O$. Fig. 2d and e show the changes of Fe 2p before and after the adsorption, respectively. The Fe–O peaks are at 711.7 and 724.3 eV (before adsorption) and 712.0 and 725.6 eV (after

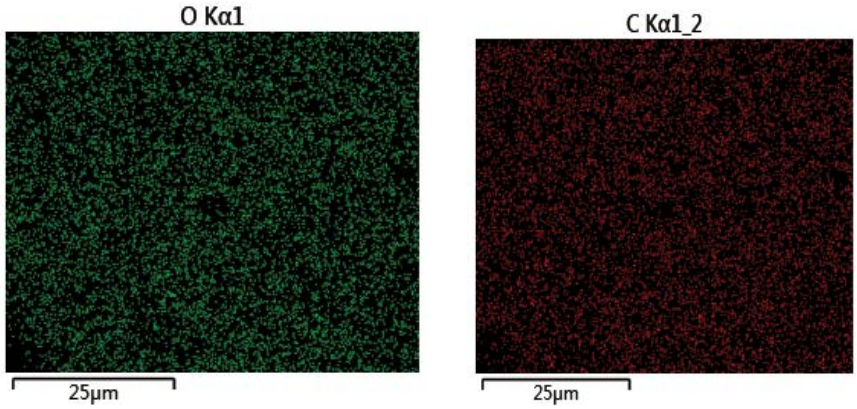


Fig. 1. Mapping of (a) O and (b) C distribution.

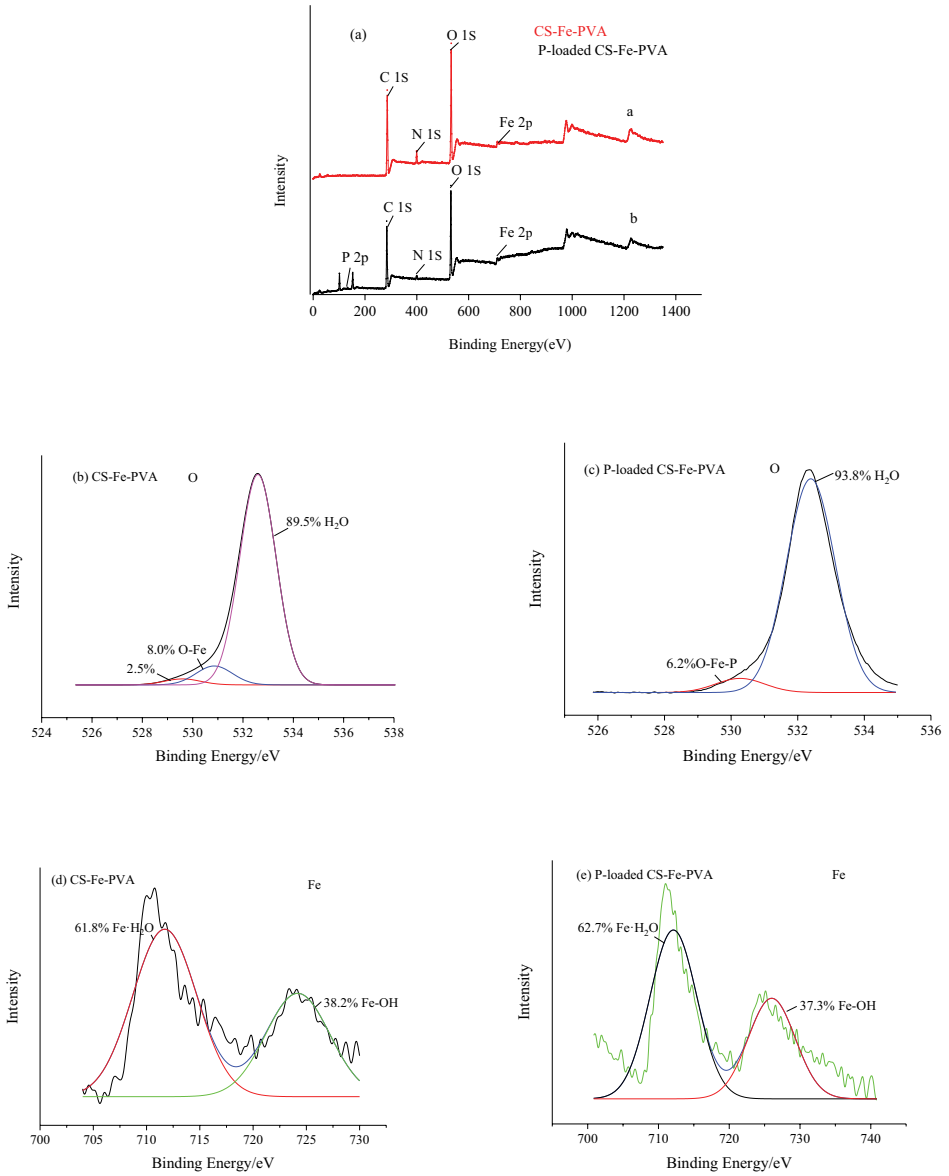


Fig. 2. XPS of CS-Fe-PVA composite membranes before and after $PO_4^{3-}$ adsorption (a). The XPS of O 1s and Fe 2p before and after $PO_4^{3-}$ adsorption (b,c) and (d,e).

adsorption). The binding energy of Fe 2p increases after adsorption due to its interaction with stronger electronegative groups.

The trivalent Fe is mostly present in hydroxylated oxide (Fe–OH, near 725.0 eV), or in the form of iron hydrate (Fe·$H_2O$, near 711.4 eV) [24]. XPS results show that Fe–OH plays a major role in the adsorption process, concluding that coordination be the major role during the adsorption process.

### 3.1.3. Zero point charge analysis

The zero point charge ($pH_{pzc}$) can show the charged state of the material surface in the solution at different pH values. The determination of $pH_{pzc}$ is helpful to choose a better adsorption condition. The results for determination of $pH_{pzc}$ are shown in Fig. 3b. It is obviously found from Fig. 3b that the $pH_{pzc}$ of CS-Fe-PVA is about 7.00, signifying that below this value the surface of CS-Fe-PVA is positively charged, which is conducive to the adsorption of anions ($PO_4^{3-}$) due to electrostatic attraction.

### 3.1.4. Fourier-transform infrared spectroscopy analysis

Fourier-transform infrared spectroscopy (FTIR) analysis can offer the information of functional groups on the surface of materials. In this experiment, KBr powder is added to the composite membranes (before and after adsorption process), and then it is made into pressed tablets for determination. FTIR spectrum of CS, CS-Fe-PVA and P-loaded CS-Fe-PVA are presented in Fig. 3a. The peaks observed in CS are mainly attributed to vibrations of –OH, $–NH_2$, C=O [15,18]. The absorption peak at 3,440 $cm^{-1}$ represents the vibration of –OH (existing in PVA and CS) and $–NH_2$ (existing in CS) vibration, and 2,923 $cm^{-1}$ peak is ascribed to $–CH_2$ vibration. The peak at 1,635 $cm^{-1}$ is the result of C=O tensile vibration in $–CONH_2$. The peak at 1,382 $cm^{-1}$ is due to bending vibration of C–H. The absorption bands of Fe–O bond located at 509 $cm^{-1}$ were recorded from FTIR of CS-Fe-PVA and P-loaded CS-Fe-PVA in Fig. 3a.

The peak of –OH at 3,436 $cm^{-1}$ was enhanced after $PO_4^{3-}$ adsorption as a result of the coordination between hydroxyl and metal after phosphate adsorption [15]. The peak vibration at 1,076 $cm^{-1}$ is ascribed to vibration of C–N, and the absorption peak position is shifted and enhanced after adsorption.

Based on the results from the characterization studies, it is inferred that Fe and chitosan be successfully introduced into the PVA membrane.

## 3.2. Batch adsorption analysis

### 3.2.1. Effect of solution pH on adsorption quantity

Solution pH plays a significant role in the adsorption process as it can affect the surface property of materials and

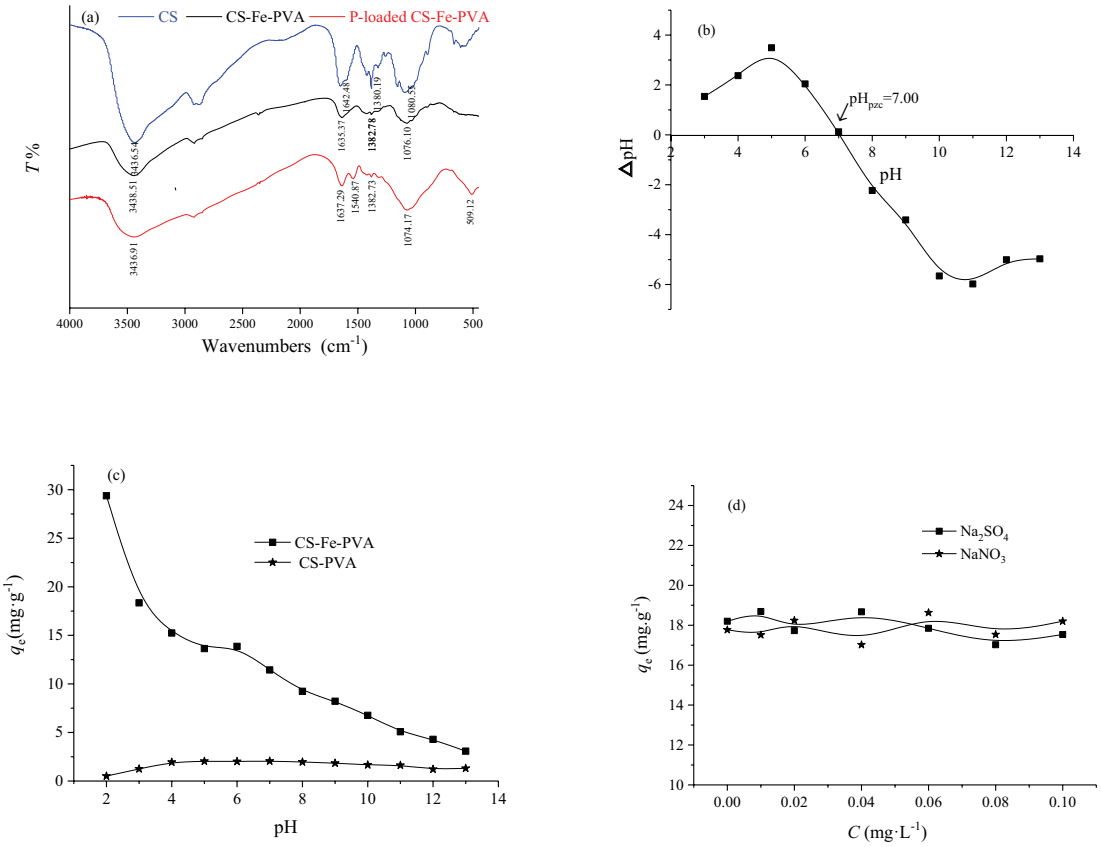


Fig. 3. (a) FTIR of CS, CS-Fe-PVA and P-loaded CS-Fe-PVA, (b) measurement of $pH_{pzc}$, (c) Effect of solution pH on phosphate adsorption, and (d) Effect of salt concentration on adsorption.

adsorbate species. The results obtained from assessing the effect of solution pH on the adsorption process are depicted in Fig. 3c. It is clearly observed from Fig. 3c that there is significant effect of solution pH on the adsorption quantity. When the solution pH is increased from 2 to 13, the $q_e$ of CS-Fe-PVA for $PO_4^{3-}$ decreases from 29.6 to 2.6 mg $g^{-1}$. This observation can be ascribed to the forms of phosphate that appear at different solution pH and the surface charge of adsorbent. There are two main forms of phosphate in solution: $H_2PO_4^-$ and $HPO_4^{2-}$ [25]. When the pH values of the adsorption environment is in the range of 2–7, the surface of CS-Fe-PVA is positively charged by protonation, and there is electrostatic interaction between the adsorbent and $H_2PO_4^-$. However, when the pH value increases, the surface of CS-Fe-PVA becomes negatively charged and repels $HPO_4^{2-}$. Also there is a competitive adsorption between $OH^-$ with $HPO_4^{2-}$ in the solution at higher solution pH. The combined effect of these factors can reduce the adsorption capacity [26,27]. Thus the pH of $PO_4^{3-}$ solution was adjusted to 3 in subsequent experiments.

It is also seen from Fig. 3c that under the same pH values, the $q_e$ of CS-Fe-PVA for the uptake of $PO_4^{3-}$ is greater than that of CS-PVA. This corroborates the significant role of Fe doping for removal of $PO_4^{3-}$. Also, the $q_e$ values of CS-PVA for $PO_4^{3-}$ are increased gradually as solution pH increased, albeit less than 2 mg $g^{-1}$. The reason for this phenomenon is that CS-PVA composite membranes may dissolve in acid environment. When the pH increases, the dissolution of CS-PVA composite membranes is ameliorated and the adsorption capacity rises. Therefore, it can be implied that Fe doping can also increase the stability of the composite membranes in acidic environment.

### 3.2.2. Influence of coexisting ions for adsorption

Normally, wastewater that is released into the environment contains some common ions. So it is necessary to study the effect of coexisting ions on the adsorption quantity. The experimental results from this assessment using $Na_2SO_4$ and $NaNO_3$ are presented in Fig. 3d. As shown in Fig. 3d, the change of $q_e$ is not significant (values of $q_e$, 17.0–19.0 mg $g^{-1}$). This confirmed that $PO_4^{3-}$ ions are well bonded to the surface of CS-Fe-PVA during the adsorption process and are less influenced by the coexisting salt ions. This confirms that electrostatic attraction is not the main mechanism. The same phenomenon has been observed in another study [28].

### 3.2.4. Effect of contact time on adsorption

Kinetic study is also important during adsorption process. The effect of contact time on the adsorption quantity are presented in Fig. 4a–c at different initial concentrations and temperature.

It is obviously seen from Fig. 4 that the adsorption kinetic curve of CS-Fe-PVA increases continuously at the initial stages; then the trend begins to slow down until

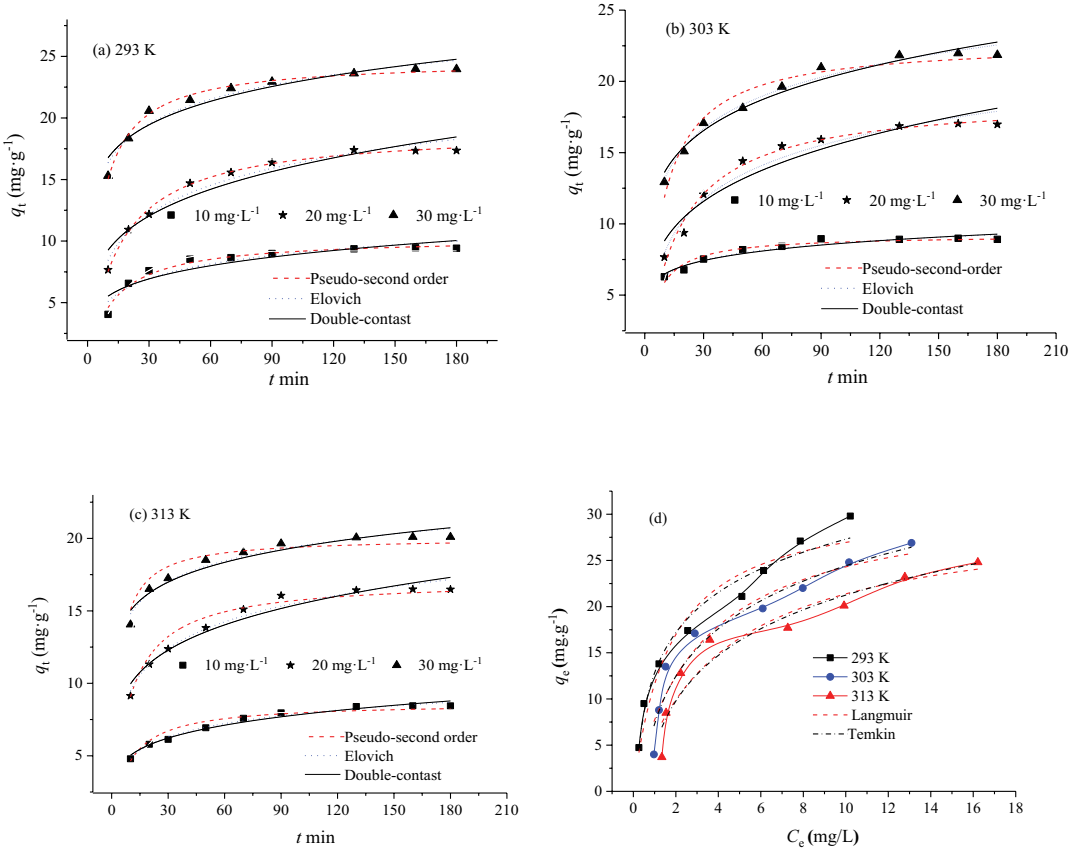


Fig. 4. Kinetic curves at 293 K (a), 303 K (b) and 313 K (c); adsorption isotherm curves (d).

the curve reaches equilibrium. This is due to accessibility of active sites and adsorbate molecules at the initial stage which leads to a higher concentration gradient. However, as the adsorption proceeds, the number of active sites become gradually occupied by the adsorbate as a result the speed of adsorption became lower until the equilibrium is attained. With the increase of reaction temperatures (at the same concentration of $PO_4^{3-}$ solution), the adsorption quantity of the composite membranes toward $PO_4^{3-}$ is observed to decrease simultaneously, signifying the process to be an exothermic reaction.

Three kinetic models, the pseudo-second-order kinetic model, Elovich equation and double constant equation, were fitted to the kinetic data for the adsorption of $PO_4^{3-}$ onto CS-Fe-PVA. Using nonlinear regressive analysis, the fitted results and curves were shown in Table 1 and in Fig. 4a–c, respectively.

Pseudo-second-order kinetic model can be applied to determine whether the process is dominated by either physical or chemical forces. The Elovich equation represents the heterogeneous adsorption of ion exchange system. The results in Table 1 show that there are the largest values of $R^2$ values and smallest values of SSE about pseudo-second-order kinetic model. Furthermore, the fitted curves from this model are very close to the experimental points. This implies that pseudo-second-order kinetic model is best to predict the kinetic process. Therefore, the adsorption of $PO_4^{3-}$ onto CS-Fe-PVA may be significantly controlled by chemical forces. It is also observed that there are smaller SSE and higher values of $R^2$ (over 0.9) about Elovich equation and

Table 1
Kinetic fitting results of adsorption of $PO_4^{3-}$ by CS-Fe-PVA composite membranes

| Pseudo-second-order kinetic model | | | | | | |
|---|---|---|---|---|---|---|
| $T$ (K) | $C_0$ (mg $L^{-1}$) | $q_{e(exp)}$ (mg $g^{-1}$) | $q_{e(theo)}$ (mg $g^{-1}$) | $k_2 \times 10^{-3}$ | $R^2$ | SSE |
| 293 | 10.0 | 9.51 | 10.3 ± 0.20 | 7.87 ± 0.92 | 0.974 | 0.084 |
| | 20.0 | 17.4 | 19.1 ± 0.19 | 3.42 ± 0.18 | 0.995 | 0.061 |
| | 30.0 | 23.9 | 24.7 ± 0.16 | 6.31 ± 0.33 | 0.991 | 0.0800 |
| 303 | 10.0 | 8.82 | 9.21 ± 0.15 | 19.2 ± 2.6 | 0.933 | 0.0698 |
| | 20.0 | 17.1 | 18.9 ± 0.35 | 3.16 ± 0.31 | 0.983 | 0.201 |
| | 30.0 | 22.0 | 22.8 ± 0.46 | 4.75 ± 0.64 | 0.951 | 0.521 |
| 313 | 10.0 | 8.51 | 8.65 ± 0.014 | 13.4 ± 0.20 | 0.922 | 0.0510 |
| | 20.0 | 16.4 | 17.1 ± 0.029 | 6.56 ± 0.096 | 0.924 | 0.201 |
| | 30.0 | 20.1 | 20.0 ± 0.021 | 15.2 ± 0.027 | 0.838 | 0.156 |
| Elovich equation | | | | | | |
| $T$ (K) | $C_0$ (mg $L^{-1}$) | | $A$ | $B$ | $R^2$ | SSE |
| 293 | 10.0 | | 1.16 | 1.70 | 0.882 | 0.377 |
| | 20.0 | | 0.60 | 3.40 | 0.965 | 0.413 |
| | 30.0 | | 9.71 | 2.88 | 0.944 | 0.484 |
| 303 | 10.0 | | 4.05 | 1.00 | 0.940 | 0.628 |
| | 20.0 | | 0.131 | 3.45 | 0.955 | 0.546 |
| | 30.0 | | 5.57 | 3.27 | 0.981 | 0.207 |
| 313 | 10.0 | | 1.74 | 1.34 | 0.985 | 0.0264 |
| | 20.0 | | 3.36 | 2.66 | 0.970 | 0.211 |
| | 30.0 | | 10.1 | 2.04 | 0.948 | 0.222 |
| Double constant equation | | | | | | |
| $T$ (K) | $C_0$ (mg $L^{-1}$) | | $A$ | $K_s$ | $R^2$ | SSE |
| 293 | 10.0 | | 3.43 ± 0.58 | 0.207 ± 0.038 | 0.817 | 0.584 |
| | 20.0 | | 5.34 ± 0.67 | 0.239 ± 0.028 | 0.918 | 0.959 |
| | 30.0 | | 12.3 ± 0.82 | 0.135 ± 0.015 | 0.914 | 0.914 |
| 303 | 10.0 | | 4.86 ± 0.29 | 0.125 ± 0.014 | 0.951 | 0.0837 |
| | 20.0 | | 4.94 ± 0.69 | 0.250 ± 0.031 | 0.920 | 1.09 |
| 313 | 30.0 | | 9.03 ± 0.52 | 0.178 ± 0.013 | 0.910 | 0.393 |
| | 10.0 | | 3.23 ± 0.18 | 0.192 ± 0.013 | 0.970 | 0.0536 |
| | 20.0 | | 6.41 ± 0.51 | 0.191 ± 0.018 | 0.942 | 0.414 |
| | 30.0 | | 11.6 ± 0.59 | 0.111 ± 0.012 | 0.925 | 0.323 |

*Notes*: SSE = $\sum (q - q_e)^2$, $q$ and $q_c$ are the experimental value and calculated value according the model, respectively.

double constant equation. This suggests that the adsorption of $PO_4^{3-}$ onto CS-Fe-PVA be attributed to chemical adsorption and heterogeneous diffusion.

### 3.2.5. Adsorption isotherm curves

The effect of adsorbate concentration on adsorption quantity is performed at various temperatures and the results are shown in Fig. 4d (isotherm curves). It is clearly noticed from Fig. 4d that the values of $q_e$ increase with the increase of $C_e$ while the curve has a steeper slope at the initial stage. When the temperature increased from 293 to 313 K, the values of $q_e$ are slightly decreased from 23.9 to 20.1 mg $g^{-1}$. This also shows that adsorption process is exothermic.

Langmuir model and Temkin model are used to explore the results of adsorption of $PO_4^{3-}$ onto CS-Fe-PVA at 293, 303 and 313 K. The results of nonlinear fitting are shown in Table 2 whereas the fitted curves are also presented in Fig. 4d. Langmuir model implies that the adsorbent is not a complex multilayer structure but a simple monolayer structure, and the capabilities at all positions where adsorption occurs are equivalent. Temkin model indicates whether there is uneven surface adsorption in the adsorption process. In Table 2, the $R^2$ value from Langmuir model are greater than 0.9, and the SSE value is smaller. At the same time, the $K_L$ value from Langmuir model becomes smaller with the rise of temperature.

The values of $R^2$ from Temkin model are also higher than 0.9 at the studied temperatures, while the values of SSE are relatively smaller. This implies that the adsorption of $PO_4^{3-}$ onto CS-Fe-PVA also conforms to Temkin model. It is concluded that the adsorption of CS-Fe-PVA for $PO_4^{3-}$ occurs via an uneven surface adsorption with single molecular layer. It is also observed that the fitted curves from both models are close to experimental curves. So the equilibrium process can be predicted using Langmuir model and Temkin model.

The adsorption capacity of CS-Fe-PVA toward $PO_4^{3-}$ is compared to other adsorbents and the data are shown in Table 3. The adsorption capacity is affected by several factors, such as acidity, salinity and temperature. However the adsorption capacity of adsorbents towards specific pollutants can be judged directly from values of adsorption quantity. It is directly observed from Table 3 that there is good adsorption capacity of CS-Fe-PVA for removal of $PO_4^{3-}$. So there is some competitive advantage in its potential for practical application.

### 3.2.6. Thermodynamic parameters of adsorption

Thermodynamic parameters, including $\Delta H°$, $\Delta G°$ and $\Delta S°$, can be determined using the following equations [37].

$$K_c = \frac{C_{ad,e}}{C_e} \tag{7}$$

$$\Delta G° = -RT \ln K_c \tag{8}$$

$$\Delta G° = \Delta H° - T\Delta S° \tag{9}$$

where $K_c$ is the coefficient of adsorption, $C_{ad,e}$ (mg $L^{-1}$) is the concentration of phosphate on CS-Fe-PVA at equilibrium, $R$ (8.314 J $mol^{-1}$ $K^{-1}$) and $T$ (K) are the universal gas constant and absolute temperature.

The activation energy ($E_a$) for phosphate adsorption is obtained by the Arrhenius equation:

$$\ln k_2 = \ln k_0 - \frac{E_a}{RT} \tag{10}$$

where $k_0$ (g $mg^{-1}$ $min^{-1}$) is the temperature independent factor.

Then the thermodynamic parameters can be calculated. Values of $\Delta G°$ are –7.03, –3.57, –2.64 kJ $mol^{-1}$ at 293, 303, and 313 K, respectively, signifying the adsorption process to be spontaneous with the spontaneity of the adsorption process decreasing with an increase in temperature. The exothermic nature of the adsorption process is corroborated by the obtained $\Delta H°$ value (i.e., –70.9 kJ $mol^{-1}$). The magnitude of the $\Delta H°$ value confirms the process to be chemical adsorption. The negative value of $\Delta S°$ (–0.220 kJ $mol^{-1}$ $K^{-1}$) indicates that the degree of disorderliness at the solid/liquid interface

Table 2
Results of isotherm nonlinear fitting of the adsorption of $PO_4^{3-}$ by CS-Fe-PVA

| Langmuir | | | | | |
|---|---|---|---|---|---|
| $T$ (K) | $q_{m(exp)}$ (mg $g^{-1}$) | $q_{m(theo)}$ (mg $g^{-1}$) | $K_L$ (L $mg^{-1}$) | $R^2$ | SSE |
| 293 | 29.8 | 31.6 ± 2.7 | 0.579 ± 0.17 | 0.928 | 5.43 |
| 303 | 26.9 | 31.9 ± 3.3 | 0.319 ± 0.095 | 0.911 | 5.54 |
| 313 | 24.8 | 30.1 ± 3.2 | 0.244 ± 0.073 | 0.908 | 4.81 |
| Temkin | | | | | |
| $T$ (K) | $A$ | $B$ | | $R^2$ | SSE |
| 293 | 12.8 ± 0.80 | 6.29 ± 0.52 | | 0.954 | 3.44 |
| 303 | 7.30 ± 1.28 | 7.44 ± 0.79 | | 0.926 | 4.61 |
| 313 | 4.83 ± 1.71 | 7.13 ± 0.79 | | 0.921 | 4.12 |

Table 3
Comparison of the adsorption properties of $PO_4^{3-}$ by various adsorbents

| Adsorbents | $q_m$ (mg $g^{-1}$) | References |
|---|---|---|
| Fe-IDA magnetic peanut husk | 33.7 | [25] |
| Al-IDA magnetic peanut husk | 16.8 | [29] |
| Zr/Al-montmorillonite | 18.1 | [30] |
| Iron zirconium oxide | 13.7 | [31] |
| La modified chelating resin | 26.1 | [32] |
| $Fe_2O_3$ nanoparticles | 5.03 | [33] |
| Innovative modified bentonites | 11.2 | [34] |
| La-impregnated zeolite | 7.45 | [35] |
| Zr-PEI@$Fe_3O_4$ | 16.4 | [36] |
| CS-Fe-PVA | 29.8 | This study |

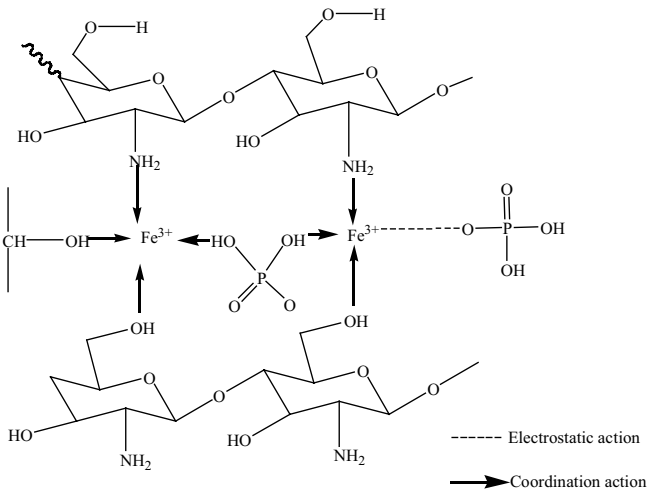


Fig. 5. Mechanism for $PO_4^{3-}$ adsorption onto CS-Fe-PVA.

during the adsorption process decreases with the rise of the temperature. The obtained $E_a$ value (13.2 kJ mol$^{-1}$) indicates the likelihood of physical forces in the adsorption process.

### 3.2.7. Desorption

Reuse of adsorbate-loaded adsorbent can make the treatment process economical thus it is necessary to regenerate and reuse the exhausted adsorbent, or recover the valuable compounds [38–40]. The efficiency of desorption using 0.1 mol L$^{-1}$ NaOH solution is 85%. This shows that the phosphate loaded on adsorbate is recovered from the solution. Similar result was obtained about regeneration of phosphate loaded UiO-66-$NH_2$ using NaOH solution [25,28,41].

## 3.3. Adsorption mechanism

Based on the results from the experiments and subsequent analysis, the adsorption of $PO_4^{3-}$ onto CS-Fe-PVA is dominated by single molecular layer adsorption on an uneven surface. According to results of the thermodynamic analysis, the uptake of $PO_4^{3-}$ onto CS-Fe-PVA proceeded via both physical and chemical adsorption processes. There should be electrostatic attraction involved in the adsorption process from the effect of solution pH on adsorption quantity. XPS results showed that Fe–OH plays a major role in the adsorption process, indicating coordination mechanism in the process. Of course, there may be hydrogen-bond between –OH or $^-NH_2$ from CS and $H_2PO_4^-$ [25,42]. From these results, the plausible adsorption mechanism underlying the adsorption of $PO_4^{3-}$ onto CS-Fe-PVA is shown in Fig. 5.

## 4. Conclusion

In this study, characterization of CS-Fe-PVA membrane shows successful Fe and CS loading. Adsorption capacity is enhanced with Fe introduction. CS-Fe-PVA exhibits high stability in weak acidic condition. The adsorption of $PO_4^{3-}$ onto CS-Fe-PVA is favored under acidic conditions. There is a good adsorption capacity of CS-Fe-PVA toward phosphate. The process of $PO_4^{3-}$ uptake onto CS-Fe-PVA is spontaneous and exothermic with the coordination mechanism being the major mechanism. The results suggest that the membrane CS-Fe-PVA can be applied to removal of phosphates from solution.

## Acknowledgement

This work was supported in part by the Key Scientific Research Project in Universities of Henan Province (19A150048).

## References

[1] R.W. Howarth, R. Marino, Nitrogen as the limiting nutrient for eutrophication in coastal marine ecosystems: evolving views over three decades, Limnol. Oceanogr., 51 (2006) 364–376.
[2] B.L. Wu, J. Wan, Y.Y. Zhang, B.C. Pan, I.M.C. Lo, Selective phosphate removal from water and wastewater using sorption: process fundamentals and removal mechanisms, Environ. Sci. Technol., 54 (2020) 50–66.
[3] M.Y. Liu, Q. Liu, Z.Y. Zang, R.P. Han, Adsorptive removal of sulfosalicylic acid from aqueous medium by iron(III)-loaded magnetic chitosan/graphene oxide, J. Colloid Interface Sci., 606 (2022) 1249–1260.
[4] B. Li, M.T. Brett, The impact of alum based advanced nutrient removal processes on phosphorus bioavailability, Water Res., 46 (2012) 837–844.
[5] F.V. Hackbarth, F. Girardi, J.O.C. Santos, A.N.A.U. De Souza, R.A.R. Boaventura, S.M.A.G.U. de Souza, V.J.P. Vilar, Ion-exchange breakthrough curves for single and multi-metal systems using marine macroalgae *Pelvetia canaliculata* as a natural cation exchanger, Chem. Eng. J., 269 (2015) 359–370.
[6] E.M. Seftel, R.G. Ciocarlan, B. Michielsen, V. Meynen, S. Mullens, P. Cool, Insights into phosphate adsorption behavior on structurally modified ZnAl layered double hydroxides, Appl. Clay Sci., 165 (2018) 234–246.
[7] A.A. Aryee, F.M. Mpatani, A.N. Kani, E. Dovi, R.P. Han, Z.H. Li, L.B. Qu, A review on functionalized adsorbents based on peanut husk for the sequestration of pollutants in wastewater: modification methods and adsorption study, J. Cleaner Prod., 310 (2021) 127502, doi: 10.1016/j.jclepro.2021.127502.
[8] G. Crini, E. Lichtfouse, Advantages and disadvantages of techniques used for wastewater treatment, Environ. Chem. Lett., 17 (2019) 145–155.
[9] F.M. Mpatani, R.P. Han, A.A. Aryee, A.N. Kani, Z.H. Li, L.B. Qu, Adsorption performance of modified agricultural waste materials for removal of emerging micro-contaminant bisphenol A: a comprehensive review, Sci. Total Environ., 780 (2021) 146629, doi: 10.1016/j.scitotenv.2021.146629.
[10] X. Xu, B.Y. Gao, B. Jin, Q.Y. Yue, Removal of anionic pollutants from liquids by biomass materials: a review, J. Mol. Liq., 215 (2016) 565–595.
[11] P.S. Kumar, L. Korving, M.C.M. van Loosdrecht, G.J. Witkamp, Adsorption as a technology to achieve ultra-low concentrations of phosphate: research gaps and economic analysis, Water Res. X, 4 (2019) 100029, doi: 10.1016/j.wroa.2019.100029.
[12] G. Crini, P.M. Badot, Application of chitosan, a natural aminopolysaccharide, for dye removal from aqueous solutions by adsorption processes using batch studies: a review of recent literature, Prog. Polym. Sci., 33 (2008) 399–447.
[13] C.M. Futalan, C.C. Kan, M.L. Dalida, K.J. Hsien, C. Pascua, M.W. Wan, Comparative and competitive adsorption of copper, lead, and nickel using chitosan immobilized on bentonite, Carbohydr. Polym., 83 (2011) 528–536.
[14] M.J. Ahmed, B.H. Hameed, E.H. Hummadi, Review on recent progress in chitosan/chitin-carbonaceous material composites for the adsorption of water pollutants, Carbohydr. Polym., 247 (2020) 116690, doi: 10.1016/j.carbpol.2020.116690.
[15] M.Y. Liu, X.T. Zhang, Z.H. Li, L.B. Qu, R.P. Han, Fabrication of zirconium(IV)-loaded chitosan/$Fe_3O_4$/graphene oxide for efficient removal of alizarin red from aqueous solution,

Carbohydr. Polym., 248 (2020) 116792, doi: 10.1016/j.carbpol.2020.116792.
[16] T. Anitha, P.S. Kumar, K.S. Kumar, B. Ramkumar, S. Ramalingam, Adsorptive removal of Pb(II) ions from polluted water by newly synthesized chitosan–polyacrylonitrile blend: equilibrium, kinetic, mechanism and thermodynamic approach, Process Saf. Environ. Prot., 98 (2015) 187–197.
[17] T. Zhou, L.Y. Fang, X.W. Wang, M.Y. Han, S.S. Zhang, R.P. Han, Adsorption of the herbicide 2,4-dichlorophenoxyacetic acid by Fe-crosslinked chitosan complex in batch mode, Desal. Water Treat., 70 (2017) 294–301.
[18] K. Wen, Y. Li, S.X. Zhang, X.T. Zhang, R.P. Han, Adsorption of Congo red from solution by iron doped PVA-chitosan composite film, Desal. Water Treat., 187 (2020) 378–389.
[19] A.R. Nesic, S.J. Velickovic, D. Antonovic, Characterization of chitosan/montmorillonite membranes as adsorbents for Bezactiv Orange V-3R dye, J. Hazard. Mater., 209–210 (2012) 256–263.
[20] E. Salehi, P. Daraei, A.A. Shamsabadi, A review on chitosan-based adsorptive membranes, Carbohydr. Polym., 152 (2016) 419–432.
[21] D.E.S. Santos, C.G.T. Neto, J.L.C. Fonseca, M.R. Pereira, Chitosan macroporous asymmetric membranes—preparation, characterization and transport of drugs, J. Membr. Sci., 325 (2008) 362–370.
[22] U. Habiba, A.M. Afifi, A. Salleh, B.C. Ang, Chitosan/(polyvinyl alcohol)/zeolite electrospun composite nanofibrous membrane for adsorption of $Cr^{6+}$, $Fe^{3+}$ and $Ni^{2+}$, J. Hazard. Mater., 322 (2016) 182–194.
[23] M. Mallet, K. Barthélémy, C. Ruby, A. Renard, S. Naille, Investigation of phosphate adsorption onto ferrihydrite by X-ray photoelectron spectroscopy, J. Colloid Interface Sci., 407 (2013) 95–101.
[24] Y. Su, H. Cui, Q. Li, S.A. Gao, J.K. Shang, Strong adsorption of phosphate by amorphous zirconium oxide nanoparticles, Water Res., 47 (2013) 5018–5026.
[25] A.A. Aryee, F.M. Mpatani, X.T. Zhang, A.N. Kani, E. Dovi, R.P. Han, Z.H. Li, L.P. Qu, Iron(III) and iminodiacetic acid functionalized magnetic peanut husk for the removal of phosphate from solution: characterization, kinetic and equilibrium studies, J. Cleaner Prod., 268 (2020) 122191, doi: 10.1016/j.jclepro.2020.122191.
[26] T.J. Daou, S. Begin-Colin, J.M. Grenèche, F. Thomas, A. Derory, P. Bernhardt, P. Legaré, G. Pourroy, Phosphate adsorption properties of magnetite-based nanoparticles, Chem. Mater., 19 (2007) 4494–4505.
[27] Z.M. Ren, L.N. Shao, G.S. Zhang, Adsorption of phosphate from aqueous solution using an iron–zirconium binary oxide sorbent, Water Air Soil Pollut., 223 (2012) 4221–4231.
[28] Y.F. Gu, M.M. Yang, W.L. Wang, R.P. Han, Phosphate adsorption from solution by zirconium loaded carbon nanotubes in batch mode, J. Chem. Eng. Data, 64 (2019) 2849–2858.
[29] A.A. Aryee, E. Dovi, R.P. Han, Z.H. Li, L.B. Qu, One novel composite based on functionalized magnetic peanut husk as adsorbent for efficient sequestration of phosphate and Congo red from solution: characterization, equilibrium, kinetic and mechanism studies, J. Colloid Interface Sci., 598 (2021) 69–82.
[30] W. Huang, J. Chen, F. He, J. Tang, D. Li, Y. Zhu, Y. Zhang, Effective phosphate adsorption by Zr/Al-pillared montmorillonite: insight into equilibrium, kinetics and thermodynamics, Appl. Clay Sci., 104 (2015) 252–260.
[31] F. Long, J.L. Gong, G.M. Zeng, L. Chen, X.Y. Wang, J.H. Deng, Q.Y. Niu, H.Y. Zhang, X.R. Zhang, Removal of phosphate from aqueous solution by magnetic Fe-Zr binary oxide, Chem. Eng. J., 17 (2011) 448–455.
[32] X.T. Zhang, C.H. Ma, K. Wen, R.P. Han, Adsorption of phosphate from solution by lanthanum modified macroporous chelating resin, Korean J. Chem. Eng., 37 (2020) 776–775.
[33] S.Y. Yoon, C.G. Lee, J.A. Park, J.H. Kim, S.B. Kim, S.H. Lee, J.W. Choi, Kinetic, equilibrium and thermodynamic studies for phosphate adsorption to magnetic iron oxide nanoparticles, Chem. Eng. J., 236 (2014) 341–347.
[34] M. Zamparas, A. Gianni, P. Stathi, Y. Deligiannakis, I. Zacharias, Removal of phosphate from natural waters using innovative modified bentonites, Appl. Clay Sci., 62–63 (2012) 101–106.
[35] Y.H. He, H. Lin, Y.B. Dong, Q.L. Liu, L. Wang, Simultaneous removal of ammonium and phosphate by alkaline-activated and lanthanum-impregnated zeolite, Chemosphere, 164 (2016) 387–395.
[36] C.H. Ma, X.T. Zhang, K. Wen, R. Wang, R.P. Han. Facile synthesis of polyethyleneimine@$Fe_3O_4$ loaded with zirconium for enhanced phosphate adsorption: Performance and adsorption mechanism, Korean J. Chem. Eng., 38 (2021) 135–143.
[37] S.S. Chen, Z.Y. Zang, S.S. Zhang, G.F. Ouyang, R.P. Han, Preparation of MIL-100(Fe) and multi-walled carbon nanotubes nanocomposite with high adsorption capacity towards oxytetracycline from solution, J. Environ. Chem. Eng., 9 (2021) 104780, doi: 10.1016/j.jece.2020.104780.
[38] H.N. Bhatti, Z. Mahmood, A. Kausar, S.M. Yakout, O.H. Shair, M. Iqbal, Biocomposites of polypyrrole, polyaniline and sodium alginate with cellulosic biomass: adsorption-desorption, kinetics and thermodynamic studies for the removal of 2,4-dichlorophenol, Int. J. Biol. Macromol., 153 (2020) 146–157.
[39] J.L. Wang, X. Liu, M.M. Yang, H.Y. Han, S.S. Zhang, G.F. Ouyang, R.P. Han, Removal of tetracycline using modified wheat straw from solution in batch and column modes, J. Mol. Liq., 338 (2021) 116698, doi: 10.1016/j.molliq.2021.116698.
[40] F.M. Mpatani, A.A. Aryee, A.N. Kani, Q.H. Guo, E. Dovi, L.B. Qu, Z.H. Li, R.P. Han, Uptake of micropollutant-bisphenol A, methylene blue and neutral red onto a novel bagasse-β-cyclodextrin polymer by adsorption process, Chemosphere, 259 (2020) 127439, doi: 10.1016/j.chemosphere.2020.127439.
[41] X.T. Zhang, M.Y. Liu, R.P. Han, Adsorption of phosphate on UiO-66-$NH_2$ prepared by a green synthesis method, J. Environ. Chem. Eng., 9 (2021) 106672, doi: 10.1016/j.jece.2021.106672.
[42] A.S. Eltaweil, A.M. Omer, H.G. El-Aqapa, N.M. Gaber, N.F. Attia, G.M. El-Subruiti, M.S. Mohy-Eldin, E.M. Abd El-Monaem, Chitosan based adsorbents for the removal of phosphate and nitrate: a critical review, Carbohydr. Polym., 274 (2021) 118671, doi: 10.1016/j.carbpol.2021.118671.